

Article

Effect of the Sizing Removal Methods of Fiber Surface on the Mechanical Performance of Basalt Fiber-Reinforced Concrete

Yeou-Fong Li ^{1,*}, Jia-Yin Hung ¹, Jin-Yuan Syu ^{1,*}, Shih-Han Chen ², Chih-Hong Huang ², Shu-Mei Chang ³ and Wen-Shyong Kuo ⁴

¹ Department of Civil Engineering, National Taipei University of Technology, Taipei 10608, Taiwan; naomi6823@gmail.com

² College of Design, National Taipei University of Technology, Taipei 10608, Taiwan; shih_han669@yahoo.com (S.-H.C.); huangch@ntut.edu.tw (C.-H.H.)

³ Department of Molecular Science and Engineering, Research and Development Center for Smart Textile Technology, National Taipei University of Technology, Taipei 10608, Taiwan; f10914@mail.ntut.edu.tw

⁴ Department of Aerospace and Systems Engineering, Feng Chia University, Taichung 40724, Taiwan; wskuo@fcu.edu.tw

* Correspondence: yfli@mail.ntut.edu.tw (Y.-F.L.); t9679010@ntut.org.tw (J.-Y.S.)

Abstract: In this study, comprehensive analyses were used to evaluate the physical and chemical properties of basalt fibers, employing a variety of instruments. Additionally, heat treatment and solvent treatment methods were used to eliminate the sizing present on fiber surfaces. The heat treatment process involved determining the optimal temperature and duration required to remove the sizing from the basalt fibers. The appearance, chemical composition, and crystal structure of the original fibers were examined, including those subjected to heat treatment and those treated with solvents. These treated fibers were then incorporated into concrete to create basalt fiber-reinforced concrete (BFRC) specimens for mechanical tests, which assessed their compressive, flexural, and splitting tensile strengths. The results revealed that heat treatment at 300 °C for 180 min effectively removed the sizing on the basalt fibers, and the heat-treated basalt fibers exhibited uniform dispersion inside the BFRC specimens. In addition, solvent treatment primarily removed the soluble components of the sizing. The mechanical properties of specimens with sizing-removed basalt fibers were better than the specimens with original basalt fibers and the benchmark specimens. Crucially, the mechanical test results demonstrated that BFRC incorporating heat-treated basalt fibers exhibited a superior mechanical performance compared to BFRC incorporating original fibers or fibers subjected to the solvent treatment.

Keywords: basalt fiber; sizing; heat treatment; solvent treatment; mechanical test



Citation: Li, Y.-F.; Hung, J.-Y.; Syu, J.-Y.; Chen, S.-H.; Huang, C.-H.; Chang, S.-M.; Kuo, W.-S. Effect of the Sizing Removal Methods of Fiber Surface on the Mechanical Performance of Basalt Fiber-Reinforced Concrete. *Fibers* **2024**, *12*, 10. <https://doi.org/10.3390/fib12010010>

Academic Editor: Constantin Chalioris

Received: 31 October 2023
Revised: 29 December 2023
Accepted: 10 January 2024
Published: 15 January 2024



Copyright: © 2024 by the authors. Licensee MDPI, Basel, Switzerland. This article is an open access article distributed under the terms and conditions of the Creative Commons Attribution (CC BY) license (<https://creativecommons.org/licenses/by/4.0/>).

1. Introduction

Concrete is a composite material with low tensile strength and tensile strain limits. Adding fiber to concrete can enhance its flexural strength, tensile strength, impact resistance, toughness, and abrasion resistance [1,2]. Fiber-reinforced concrete (FRC) has been widely used in infrastructure, road construction, bridges, and offshore platforms [3,4]. In accordance with previous research, the addition of fibers to concrete necessitates careful consideration of various factors, including the fineness modulus (FM) of the aggregate, fiber type, fiber length, the amount of fiber added, the dispersion of fibers in concrete, and the bonding between the fibers and concrete [5–9].

Incorporating fibers into concrete can effectively suppress the formation and propagation of cracks, as it significantly mitigates concrete shrinkage [10,11]. Fiber lengths suitable for concrete varies with aggregate size. Fibers of 6 mm enhance the compressive strength of FRC, but 24 mm fibers bolsters the flexural strength of FRC [12–14]. Previous research indicates that adding fibers within the range of 0.75% to 1% (*w/w*) results in the most

substantial improvement in the mechanical properties of concrete. For example, adding 1% carbon fibers or Kevlar fibers with a length of 24 mm to concrete can increase the compressive and flexural strengths of fiber concrete by 4.4–39% and 27–38%, respectively, compared with plain concrete [15–17]. Hybrid fiber-reinforced concrete (HFRC), incorporating two or more types of fibers, demonstrates significantly improved static and dynamic behavior compared to single fiber-reinforced concrete. These hybrid fibers comprise various materials, including polypropylene, steel, glass, cellulose, carbon, aramid, and sisal fibers. Their combined use augments the energy absorption capacity, thereby improving impact resistance across varying water–cement ratios, and volume or weight fractions [18–22].

Common fibers used to reinforce concrete include carbon, steel, glass, basalt, and polypropylene. Among these fibers, basalt fiber has a production process and composition similar to glass fiber, but it possesses better physical properties and is less expensive than carbon fiber [5,6]. Basalt fiber is an inorganic material made from natural basalt rocks that are melted at temperatures ranging from 1500 °C to 1700 °C through the spinneret method [7,8]. In the manufacturing process, the surfaces of fibers are coated with a sizing layer to improve its ability to be processed. The sizing consists of a film former, a coupling agent, and a lubricant, with the film former accounting for approximately 80 wt% of the total mass of the sizing [23–25]. The film former is a low-molecular-weight material, while the coupling agents are typically called silane coupling agents, which are siloxane compounds known for their high hydrolysis resistance [26,27].

The presence of sizing on the surfaces of fibers can affect the mechanical behavior of fiber-reinforced composites. Cement matrix composite specimens with sizing-removed carbon fibers can attain higher compressive strengths compared to untreated carbon fiber cement matrix composite specimens [28–30]. The sizing-removed fibers can be easily dispersed in the cementitious composite, and the bonding between the fibers and the cement can be notably improved. Common sizing removal methods include heat treatment and solvent treatment. With the heat treatment method, most of the sizing can be decomposed from the surfaces of glass fibers and basalt fibers at about 300 °C, causing a decrease in the tensile force of the fiber filaments due to the removal of the sizing [31–35].

Certain studies have indicated that solvent treatments can efficiently eliminate the surface sizing of glass fibers without compromising the mechanical strength of the GFRP [36]. Solvent treatment could remove the soluble sizing, which accounts for 70% to 80% of the total sizing, from the fibers' surfaces. The results of spectroscopy and elemental analysis show that the soluble sizing is composed of film formers and other agents, while the insoluble sizing might contain silane [37–42].

The objective of this study is to investigate the influence of the surface treatment of basalt fibers on the mechanical behavior of fiber-reinforced concrete. To remove the sizing, both the heat-treated and solvent-treated methods were employed. The target temperature and holding time for the heat treatment method were determined based on thermogravimetric analysis (TGA). The soluble chemical composition of the sizing on the surface of basalt fibers was also analyzed using gas chromatography with mass spectrometry (GC/MS). In addition, tests were conducted to assess the appearance, elemental composition, crystal structure, and filament tensile force of the basalt fibers. The compressive, flexural, splitting tensile strength of basalt fiber-reinforced concrete (BFRC) specimens with the original, heat-treated, and solvent-treated basalt fibers were obtained.

2. Material and Method

This section describes the research method for assessing the physical and chemical properties of basalt fibers before and after surface treatment. Additionally, the tensile force–displacement relationship of the basalt filaments was obtained through a tensile test. According to a previous study [35], the overall mechanical properties of BFRC with basalt fibers 24 mm in length were better than with basalt fibers that were 6 mm and 12 mm long, especially in regard to flexural strength, tensile strength, and impact resistance. Furthermore, the mechanical properties of BFRC with a ratio of 1% for fiber to cement was

better than with 0.5% and 1.5%; thus, 1% chopped basalt fibers of 24 mm (Sheng Peng Applied Materials Co., Ltd., Yunlin County, Taiwan) was used in this study. The linear density and diameters of the basalt fibers used in this study were 300 tex and $11.7 \pm 1.93 \mu\text{m}$ ($N = 15$), respectively. Figure 1 displays the appearance of the basalt fibers.

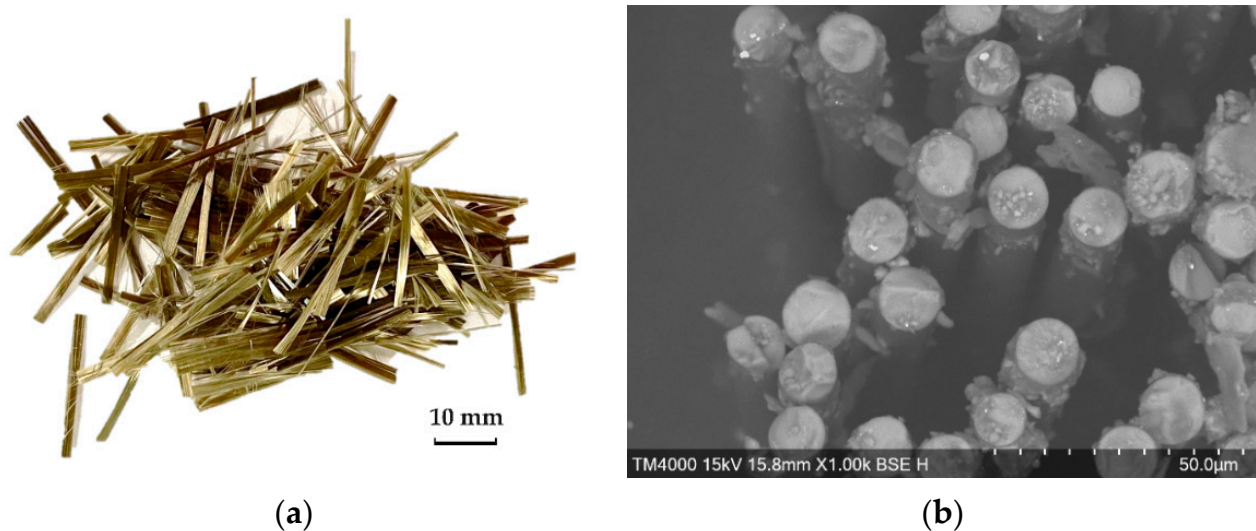


Figure 1. Photo of basalt fibers (a) basalt fiber tows; and (b) cross-section of original basalt fibers by SEM (1000 \times).

2.1. Surface Treatment of Basalt Fibers

The heat treatment method and the solvent treatment method were used to remove the sizing from the surfaces of basalt fibers, and the treated fibers were then added to the concrete for reinforcement. The physical–chemical properties of the original, heat-treated, and solvent-treated basalt fibers were observed and analyzed using thermogravimetric analysis (TGA), scanning electron microscope (SEM), energy-dispersive X-ray spectroscopy (EDS), and X-ray diffractometer (XRD); a filament tensile test was also performed.

2.1.1. Heat Treatment

In order to analyze the treatment temperature and time of the basalt fibers in the heat treatment method, a TGA (SDTA851e, Mettler Toledo, Greifensee, Switzerland) was performed. Nitrogen was used as a protection gas with a flow rate of 30 mL/min. The sample, weighing about 20 mg, was placed in an alumina ceramic crucible, and the reaction gas was zero-grade air with a flow rate of 30 mL/min. The target temperature for sizing removal was determined by the TGA, with a temperature range of 25 °C to 700 °C and a heating rate of 10 °C/min. The sample was gradually heated to the target temperature at a heating rate of 10 °C/min after being held at a 25 °C isothermal state. The temperature was maintained for a specific time before being gradually raised to 700 °C at a heating rate of 10 °C/min. The mass loss was then checked at different time points under the target temperature after determining said target temperature.

2.1.2. Solvent Treatment

The sizing on the surfaces of the basalt fibers was extracted using the solvent treatment method with isopropyl alcohol (IPA, 99.8%, Emperor Chemical Co., Ltd., Taipei City, Taiwan). The basalt fibers were first dried at 80 °C for 24 h and weighed using an electronic scale (TX223L, Shimadzu, Kyoto, Japan). Then, the basalt fibers were immersed in an IPA solution at 23 °C for 24 h and dried in an oven (KOE-270, Kotsao, New Taipei City, Taiwan) at 80 °C for 24 h to remove the solvent. After that, the mass of the basalt fibers was measured to determine the amount of surface sizing removed. Furthermore, the remaining

sizing on the treated fibers was analyzed by TGA, with a temperature range of 25 °C to 700 °C and a heating rate of 10 °C/min.

2.2. Sizing Composition Analysis of Basalt Fibers

In this study, the soluble components of the sizing on the surface of the original basalt fibers by IPA were analyzed using gas chromatography/mass spectrometry (GC/MS, 7890B/5977A, Agilent Technologies, Santa Clara, CA, USA). A capillary column (19091S-433, Agilent Technologies, Santa Clara, CA, USA) was utilized for the pending sample separations in GC, with a column length of 30 m, inner diameter of 0.25 mm, and a film thickness of 0.25 µm. Helium (He) gas was employed as the carrier gas, flowing at a rate of 1 mL/min. The ultrasonic extraction method was employed for sample preparation, wherein the basalt fibers were soaked in a toluene solution to extract the sizing, and then passed through a 13 mm PTFE syringe filter with a pore size of 0.22 µm to obtain the sample. The pending sample was injected into the GC/MS in a splitless mode with an injection volume of 1 µL and an inlet temperature of 270 °C to gasify the pending sample. The oven's initial temperature was set at 230 °C for 6 min, followed by heating to 280 °C at a heating rate of 50 °C/min and holding for 5 min. Subsequently, the oven's temperature was raised to 310 °C at the heating rate of 60 °C/min and held for 3 min.

2.3. Microscopic Observation and Analysis of Basalt Fibers

The morphologies of the original, the heat-treated, and the solvent-treated basalt fibers were examined using SEM (TM4000plus II, Hitachi High-Tech, Kyoto, Japan) with a test voltage of 15 kV. The chemical composition of the fibers was analyzed using EDS (MICS F+/X-STREAM-2, Oxford, UK). Additionally, the crystal structure of the basalt fibers was analyzed using an XRD (D2 Phaser, Bruker, Rheinstetten, Germany), with Cu K α radiation as the X-ray source and a test voltage of 30 kV. The scan step size was set at 0.02°, and the range of the 2 θ was from 10° to 80°.

2.4. Tensile Force of Basalt Filament

The tensile force and displacement of the original, the heat-treated, and the solvent-treated basalt fiber filaments were obtained by the tensile testing machine (QC-513M1, Comotech, Taichung City, Taiwan) at a tensile rate of 0.5 mm/min based on ASTM D3822-07 [43]. The loadcell capacity of the tensile testing was 300 gf. In the single-filament tensile test of this study, the fiber testing length was 25 mm. Initially, a single fiber was extracted and glued on a standard paper frame. The paper frame was used to protect the fiber from direct gripping. Both sides of the frame were cut before the test, leaving only the filament to be pulled. The load was recorded with the grip displacement. The fiber was brittlely fractured at the peak load. At least 15 pieces were tested for each type of fiber.

2.5. BFRC Test Method

The BFRC specimens were created using 24 mm chopped basalt fibers, Type I Portland cement (Taiwan Cement Corp., Taipei City, Taiwan), aggregate, and water. The aggregate's fineness modulus (F.M.) was 6.31, and the test was conducted following the ASTM C33/C33M-18 standard [44]. The weight ratio of cement to fine aggregate and coarse aggregate was set to 1:1.05:2.25, and the water–cement ratio was 0.6. The basalt fiber-to-cement weight ratio was 10‰ for the BFRC specimens. Three different types of basalt fibers were used in this study, including original, heat-treated, and solvent-treated basalt fibers. According to the TGA analysis results, the heat-treated basalt fibers were obtained from the muffle furnace (PF-40, Prema, Taipei City, Taiwan), heated at 300 °C for three hours. In addition, the solvent-treated basalt fibers were immersed in IPA solution at 23 °C for 24 h and dried in the oven at 80 °C for 24 h in order to remove the solvent. Finally, those fibers were pneumatically dispersed by an air compressor under 90 psi for one minute. The production process of the BFRC specimen was in accordance with past research [18].

The compressive, flexural, and splitting tensile tests were conducted following ASTM C39/C39M-21, ASTM C496/C496M-17, and ASTM C293/C293M-16, respectively [45–47]. All specimens were tested after 28 days of curing. Table 1 explains the naming of all specimens for the above tests. For example, HBFRC-F referred to the specimen with heat-treated basalt fibers for the flexural test.

Table 1. Material properties of carbon fiber.

Item	Naming	Description
Specimen	B	Benchmark (without fiber)
	OBFRC	BFRC with original basalt fibers
	HBFRFC	BFRC with heat-treated basalt fibers
	SBFRFC	BFRC with solvent-treated basalt fibers
Mechanical test	C	Compressive test
	F	Flexural test
	S	Splitting tensile test

3. Physical–Chemical Property Results

The surface treatment results were divided into heat treatment and solvent treatment. The test results of the heat and solvent treatments for the removal of sizing from basalt fibers are described in the following subsections. The microscopic, chemical elements, and crystal structures of the original, heat-treated, and solvent-treated basalt fibers were as follows.

3.1. Surface Treatment Results

The weight loss ratio of the basalt fibers after heat treatment and solvent treatment were shown as follows.

3.1.1. Heat Treatment

The relationship between the mass ratio and temperature of basalt fibers was analyzed using TGA and presented in Figure 2. The temperature range was set from 25 °C to 700 °C, with a heating rate of 10 °C/min. As shown in Figure 2, the basalt fibers experienced less than 0.1% mass loss below 260 °C, while the primary mass loss occurred between 260 °C and 488 °C, resulting in a total mass loss of about 1%. This indicates that the sizing of the basalt fibers began to decompose at 260 °C, which coincides with the decomposing temperature of most commercial sizing of basalt fibers, around 300 °C [33,34].

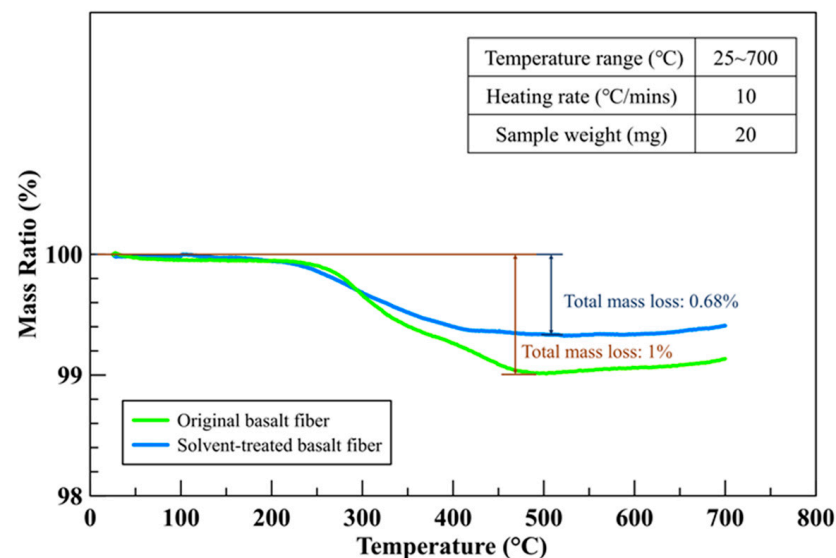


Figure 2. TGA mass ratio–temperature relationship of the basalt fibers.

Thus, a target temperature of 300 °C was chosen for sizing removal, and three different holding time durations (60, 180, and 300 min) were tested to determine the optimal heat treatment process. The mass ratio–time relationship of the 20 mg basalt fiber under different heating rates is presented in Figure 3. The mass loss for holding times of 60, 180, and 300 min at 300 °C were 0.60%, 0.68%, and 0.72%, respectively.

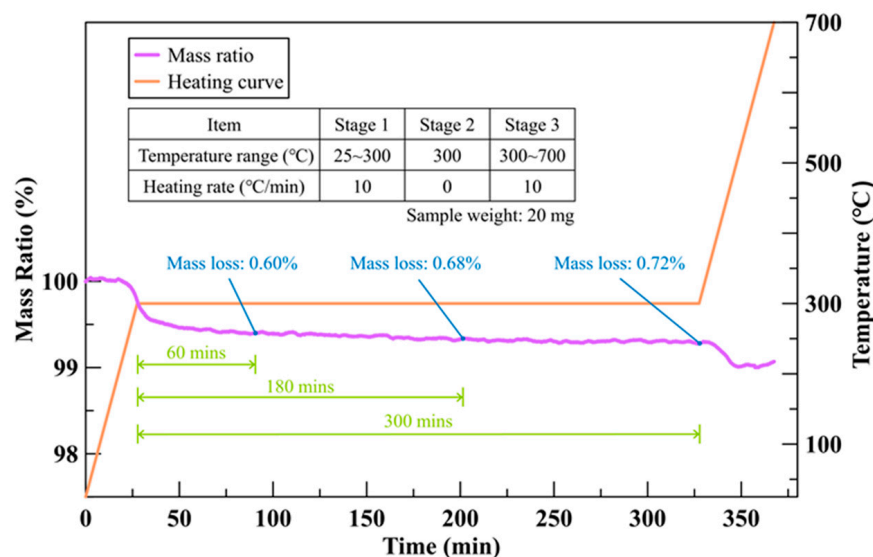


Figure 3. TGA mass ratio–time relationship of the basalt fiber.

3.1.2. Solvent Treatment

The original basalt fibers had a mass of 25.0 g, while the solvent-treated basalt fibers weighed 24.82 g, and the amount of sizing extracted from the surface of the basalt fibers was 0.7%. In order to determine the effectiveness of the solvent treatment method, the mass ratios of the 20 mg original and solvent-treated basalt fibers were tested using TGA, as shown in Figure 2. The maximum mass losses for the original and solvent-treated basalt fibers were 1% and 0.68%, respectively. Notably, the maximum mass loss for the solvent-treated basalt fibers was lower than that of the original basalt fibers, indicating that the part of the sizing was successfully extracted using the solvent-treatment method. As suggested by other researchers, parts of the sizing still remained on the surfaces of the basalt fibers after solvent extraction [48].

3.2. Sizing Composition Analysis

Figure 4 displays the chromatography of the extractive solution of the basalt fibers. In the chromatography at the 7th to 9th minutes, an unknown substance was observed to decompose at 280 °C, yielding two peaks via GC/MS. The mass-to-charge ratio and potential substance of these two unknown peaks are shown in Figures 5a and 5b, respectively. Based on the database from the NIST mass spectrometry data center, the major unknown substance in “peak A” was identified as “adipic acid, nonyl 2-octyl ester (C₂₃H₄₄O₄)”, with match factor (MF) and reverse match factor (RMF) scores of 750 and 802, respectively. This positive identification suggests it was used as an intermediate for organic synthesis, as well as in the production of lubricants, coatings, adhesives, sealants, elastomers, and other applications.

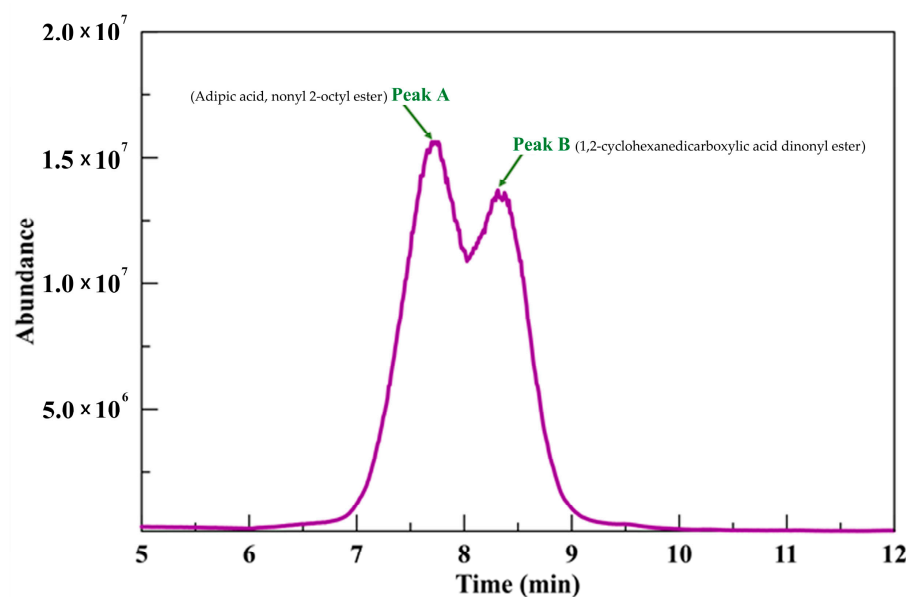


Figure 4. Chromatography of the sizing-extracted solution.

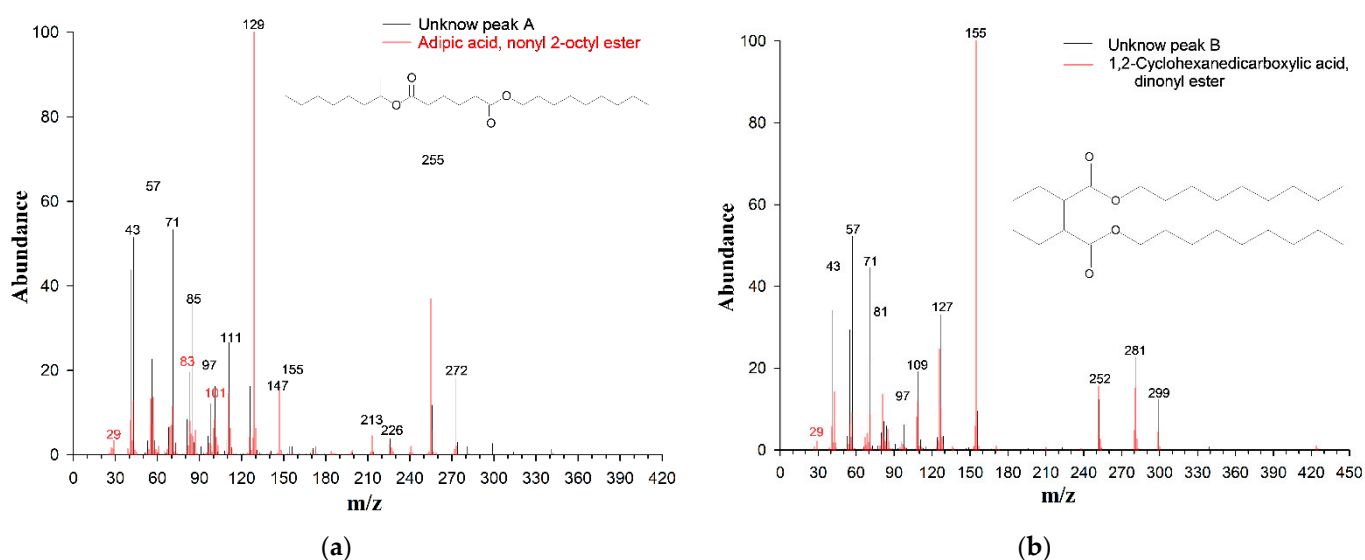


Figure 5. Chromatography of the sizing-extracted solution; (a) unknown peak A; and (b) unknown peak B.

The unknown substance in “peak B” was identified as “1,2-cyclohexanedicarboxylic acid dinonyl ester ($C_{26}H_{48}O_4$)”, with match factor (MF) and reverse match factor (RMF) scores of 832 and 856, respectively, which shows the positive identification. This substance, “1,2-cyclohexanedicarboxylic acid dinonyl ester”, is commonly used to lubricate components in plastic production.

Like most of the sizing research on fiber surfaces, this result indirectly confirmed that parts of siloxane-based addition agents were imperfectly dissolved by the organic solvent [48–50].

3.3. Microscopic Observation and Analysis

The surface morphology, chemical elements, and crystal structures of the basalt fibers were observed and analyzed using SEM, EDS, and XRD. Figure 6a–e present the SEM observations of the original basalt fibers, those heat-treated for varying durations, and the solvent-treated basalt fibers’ surface morphologies. It is evident that the original and

heat-treated basalt fibers at 300 °C for 60 min, and solvent-treated basalt fibers' surfaces, had sizing or impurities. However, sizing was removed from the surfaces of the basalt fibers by heat treatment at 300 °C for 180 and 300 min. The above results indicate that a heat treatment at 300 °C for 180 min effectively removes the sizing from the surfaces of basalt fibers. Therefore, the optimal condition for the mechanical test of the BFRC specimens was a temperature of 300 °C for 180 min. The EDS results reveal that the chemical elements present in the basalt fibers are Si, Fe, Al, Ca, and Mg, as indicated in Table 2. The weight percentage concentration of Si decreased from 25.3% to 23.7% in the original, heat-treated, and solvent-treated basalt fibers. The Si content in the basalt fibers was reduced after heat treatment. Heating the basalt fibers for longer durations could result in the growth of iron, as evidenced by an increase in iron weight percentage concentration from 8.5% to 10.7% when the heating time was 300 min.

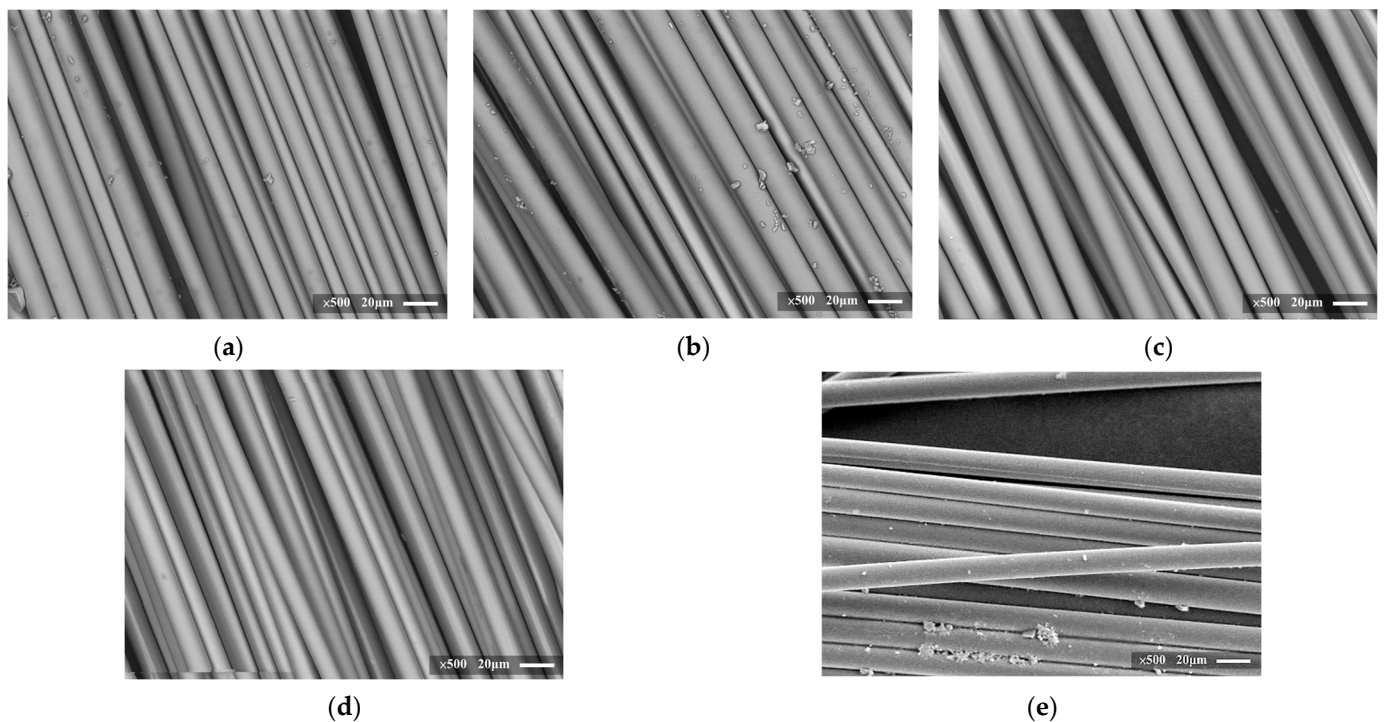


Figure 6. SEM images of the original and the surface-treated basalt fibers: (a) original; (b) heat treatment at 300 °C, 60 min; (c) heat treatment at 300 °C, 180 min; (d) heat treatment at 300 °C, 300 min; (e) solvent treatment.

Table 2. EDS results of the original, heat-treated and surface-treated basalt fibers.

Chemical Element	Original BF (wt%)	300 °C, 60 min BF (wt%)	300 °C, 180 min BF (wt%)	300 °C, 300 min BF (wt%)	Solvent-Treated BF (wt%)
O	45.3	44.2	44.1	43.2	46.6
Si	25.3	25.1	25.0	23.7	24.6
Fe	8.5	8.9	8.9	10.7	7.9
Al	8.2	8.2	8.3	8.1	7.3
Ca	5.3	5.1	5.2	5.9	5.3
Mg	3.2	3.3	3.3	3.2	2.8
Na	3.1	3.2	3.2	3.0	2.6
K	2.0	1.9	2.0	2.2	2.0

The XRD patterns of the different fibers are shown in Figure 7. The original basalt fiber specimens were amorphous, with no crystals or diffraction peaks present in the diffraction spectrum. This observation agrees with the analysis by Chakartnarodom et al. [51].

The XRD patterns of the heat-treated and solvent-treated basalt fibers showed a corresponding peak of 29.4° (2θ), indicating the presence of a crystalline phase of calcite (CaCO_3 , JCPDF-47-1743).

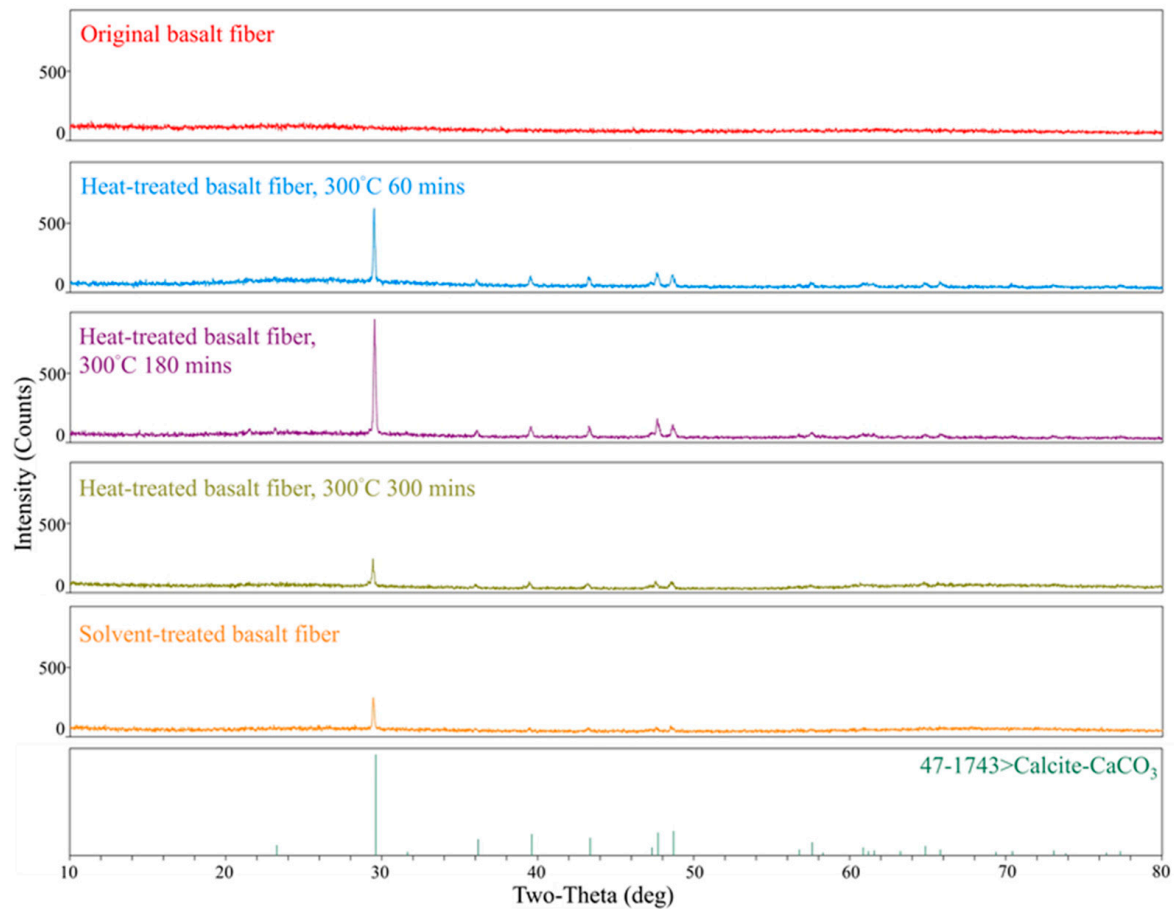


Figure 7. The XRD analysis of the original and the surface-treated basalt fibers.

3.4. Peak Tensile Force of Basalt Filament

Table 3 shows the peak tensile force and its corresponding displacement for both the original and surface-treated basalt fiber filaments. The average peak tensile force and displacement of the original filament were 22.31 gf and 0.55 mm, respectively, with corresponding standard deviations (σ) of 0.74 gf and 0.01 mm, respectively. The average peak tensile force of the heat-treated filament at 300 °C for 60, 180, and 300 min, and the solvent-treated filament were 19.00 gf, 21.76 gf, 14.60 gf, and 14.12 gf, respectively. Compared to the original filament, the heat-treated filament at 300 °C for 60 min, 180 min, and 300 min, and the solvent-treated filament experienced a decrease in the average peak tensile force of about 15%, 2%, 35%, and 37%, respectively. These results suggest that the peak tensile force of basalt fibers is affected by the heat treatment time, with longer heating times resulting in lower tensile forces.

Table 3. Peak tensile forces and displacements of the original and the surface-treated basalt fiber filaments.

No.	Original BF		300 °C, 60 min BF		300 °C, 180 min BF		300 °C, 300 min BF		Solvent-Treated BF	
	Force (gf)	Displ. (mm)	Force (gf)	Displ. (mm)	Force (gf)	Displ. (mm)	Force (gf)	Displ. (mm)	Force (gf)	Displ. (mm)
1	23.12	0.55	19.07	0.48	23.44	0.35	13.24	0.39	13.81	0.32
2	22.19	0.55	18.06	0.42	19.99	0.55	11.80	0.38	11.88	0.26
3	21.75	0.55	16.09	0.37	22.48	0.58	14.22	0.42	19.89	0.44
4	21.75	0.54	18.96	0.56	20.47	0.57	16.38	0.54	13.57	0.29
5	21.99	0.55	16.86	0.44	20.87	0.66	12.36	0.35	11.75	0.31
6	22.20	0.55	21.19	0.46	21.18	0.49	22.51	0.53	10.68	0.25
7	21.75	0.55	13.97	0.42	19.35	0.69	17.15	0.50	12.92	0.29
8	20.84	0.55	16.13	0.45	21.11	0.66	13.58	0.33	13.97	0.28
9	22.14	0.54	27.39	0.51	27.29	0.60	18.30	0.38	16.31	0.35
10	22.93	0.54	12.36	0.45	23.17	0.61	11.94	0.37	15.38	0.29
11	23.41	0.54	21.82	0.38	19.73	0.51	12.99	0.42	17.03	0.48
12	22.91	0.55	21.80	0.49	23.04	0.46	15.49	0.38	18.80	0.41
13	22.28	0.55	24.24	0.55	21.75	0.34	11.85	0.53	14.61	0.39
14	21.80	0.54	15.57	0.53	20.98	0.36	13.63	0.43	11.01	0.43
15	23.52	0.54	21.53	0.45	21.59	0.68	13.57	0.46	10.15	0.29
Avg.	22.31	0.55	19.00	0.46	21.76	0.54	14.60	0.43	14.12	0.34
σ	0.74	0.01	4.04	0.06	1.97	0.12	2.95	0.07	2.93	0.07
F value	-	-	0.033	-	0.139	-	0.062	-	0.063	-
p value	-	-	5.20×10^{-8}	-	3.59×10^{-4}	-	3.00×10^{-6}	-	3.29×10^{-6}	-
t value	-	-	3.12	-	1.00	-	9.81	-	10.50	-
p value	-	-	7.07×10^{-3}	-	3.31×10^{-1}	-	3.57×10^{-8}	-	1.38×10^{-8}	-

Force is the peak tensile force of BF filament; Displ. is the displacement of BF filament; Avg. is the average value; σ is the standard deviation.

Assuming a normal distribution for the single filament tensile forces under various conditions, with a significance level of 0.05, a sample size of 15 in a single group, and degrees of freedom amounting to 14, the analysis conducted using the F-test for variance yielded the results presented in Table 3. The p -values of the one-tailed F-test were 5.20×10^{-8} , 3.59×10^{-4} , 3.00×10^{-6} , and 3.29×10^{-6} , respectively, indicating unequal variances between the two populations. Consequently, this study proceeded with a t -test: two-sample assuming unequal variances and with a significance level of 0.05. The null hypothesis (H_0) assumed no significant difference in average value ($\mu_1 = \mu_2$), while the alternative hypothesis (H_a) suggested a significant difference in average value ($\mu_1 \neq \mu_2$). The p -values of the two-tailed t -test for “300 °C, 60 min BF”, “300 °C, 300 min BF”, and “solvent-treated BF” were 7.07×10^{-3} , 3.57×10^{-8} , and 1.38×10^{-8} , respectively. These results led to the rejection of the null hypothesis, signifying a significant difference in average values ($\mu_1 \neq \mu_2$). However, for “300 °C, 180 min BF,” the p -value of the two-tailed t -test was 3.31×10^{-1} , suggesting no significant difference in tensile strength compared to the original BF.

4. Mechanical Test of BFRC

The following section describes the materials, test methods, and mechanical test results of BFRC specimens. The specimens were made of both original and surface-treated basalt fibers, and the mechanical tests conducted were compressive, flexural, and splitting tensile tests.

4.1. Compressive Test Result

The BFRC specimens consisted of three different types of basalt fibers: original, heat-treated, and solvent-treated. Table 4 shows the compressive strengths of both the benchmark and BFRC specimens after 28 days of curing. The average compressive strengths of specimens B-C, OBFRC-C, HBFRC-C, and SBFRC-C were 23.76 MPa, 24.27 MPa, 24.44 MPa, and 25.16 MPa, respectively. The compressive strengths of the BFRC specimens increased by 2.2% for OBFRC-C, 2.9% for SBFRC-C, and 5.9% for HBFRC-C compared to the benchmark specimen.

Table 4. Compressive strength of the benchmark and the BFRC specimens.

Specimen	B-C	OBFRC-C	HBFRC-C	SBFRC-C
Compressive strength (MPa)	23.58	23.91	25.56	24.39
	22.98	24.71	24.08	24.87
	24.71	24.18	25.83	24.05
Avg. strength (MPa)	23.76	24.27	25.16	24.44
σ (MPa)	0.9	0.4	0.9	0.4

Avg. is the average value; σ is the standard deviation.

The BFRC specimens with heat-treated basalt fibers had the highest average compressive strengths among all BFRC specimens.

4.2. Flexural Test Result

Table 5 shows the flexural strength of both the benchmark and BFRC specimens after 28 days of curing. The average flexural strengths of specimens B-F, OBFRC-F, HBFRC-F, and SBFRC-F were 4.18 MPa, 4.61 MPa, 5.56 MPa and, 4.82 MPa, respectively. Compared to the benchmark specimen, the average flexural strengths of the BFRC specimens were increased by 10.2% for OBFRC-F, 15.2% for SBFRC-F, and 32.9% for HBFRC-F.

Table 5. Flexural strength of the benchmark and the BFRC specimens.

Specimen	B-F	OBFRC-F	HBFRC-F	SBFRC-F
Flexural strength (MPa)	4.03	4.68	5.30	5.16
	4.16	4.81	5.59	4.52
	4.36	4.34	5.78	4.77
Avg. strength (MPa)	4.18	4.61	5.56	4.82
σ (MPa)	0.2	0.2	0.2	0.3

Avg. is the average value; σ is the standard deviation.

The BFRC specimens with heat-treated basalt fibers had the highest average flexural strength among all specimens. Chopped basalt fibers possess toughness, whereas concrete is an inherently brittle material. These results are consistent with previous research; when combined with concrete, these fibers contribute to an increased toughness, mitigating damage due to flexural forces and minimizing crack formation in order to improve the flexural strength of concrete [2,52].

4.3. Splitting Tensile Test Result

The splitting tensile strength of the benchmark and BFRC specimens, after 28 days of curing, are listed in Table 6. The average splitting tensile strengths for each specimen were 2.57 MPa in B-S, 2.62 MPa in OBFRC-S, 2.76 MPa in HBFRC-S, and 2.67 MPa in SBFRC-S. Compared to the benchmark specimen, the average splitting tensile strengths of OBFRC-S, HBFRC-S, and SBFRC-S were improved by 2.1%, 7.4%, and 4.0%, respectively. Notably, the BFRC specimen with heat-treated basalt fibers had the highest splitting tensile strength among all specimens.

Table 6. Splitting tensile strength of the benchmark and the BFRC specimens.

Specimen	B-S	OBFRC-S	HBFRC-S	SBFRC-S
Splitting tensile strength (MPa)	2.60	2.35	2.74	2.47
	2.53	2.63	2.78	2.76
	2.20	2.89	2.74	2.78
Avg. strength (MPa)	2.57	2.62	2.76	2.67
σ (MPa)	0.2	0.2	0.02	0.2

Avg. is the average value; σ is the standard deviation.

4.4. Discussion

Based on the test results, it is evident that sizing-removed basalt fibers can improve the mechanical performance of BFRC specimens. Among the BFRC specimens, those with heat-treated basalt fibers exhibited higher mechanical strengths compared to those with the original and solvent-treated basalt fibers, as seen in Figure 6. This could be due to the absence of sizing on the surfaces of fibers, which strengthened the bonding force between the cement and the fibers. Figure 8 illustrates the different types of basalt fibers used in BFRC specimens after failure. The original fibers were difficult to disperse in concrete due to the sizing on their surfaces, while the solvent-treated basalt fibers had residual sizing, resulting in a slippage failure mode [53]. Despite the heat-treated basalt filaments achieving lower tensile force, it could be uniformly dispersed in concrete, resulting in higher mechanical strengths in the BFRC specimens compared to those with the original and solvent-treated basalt fibers.

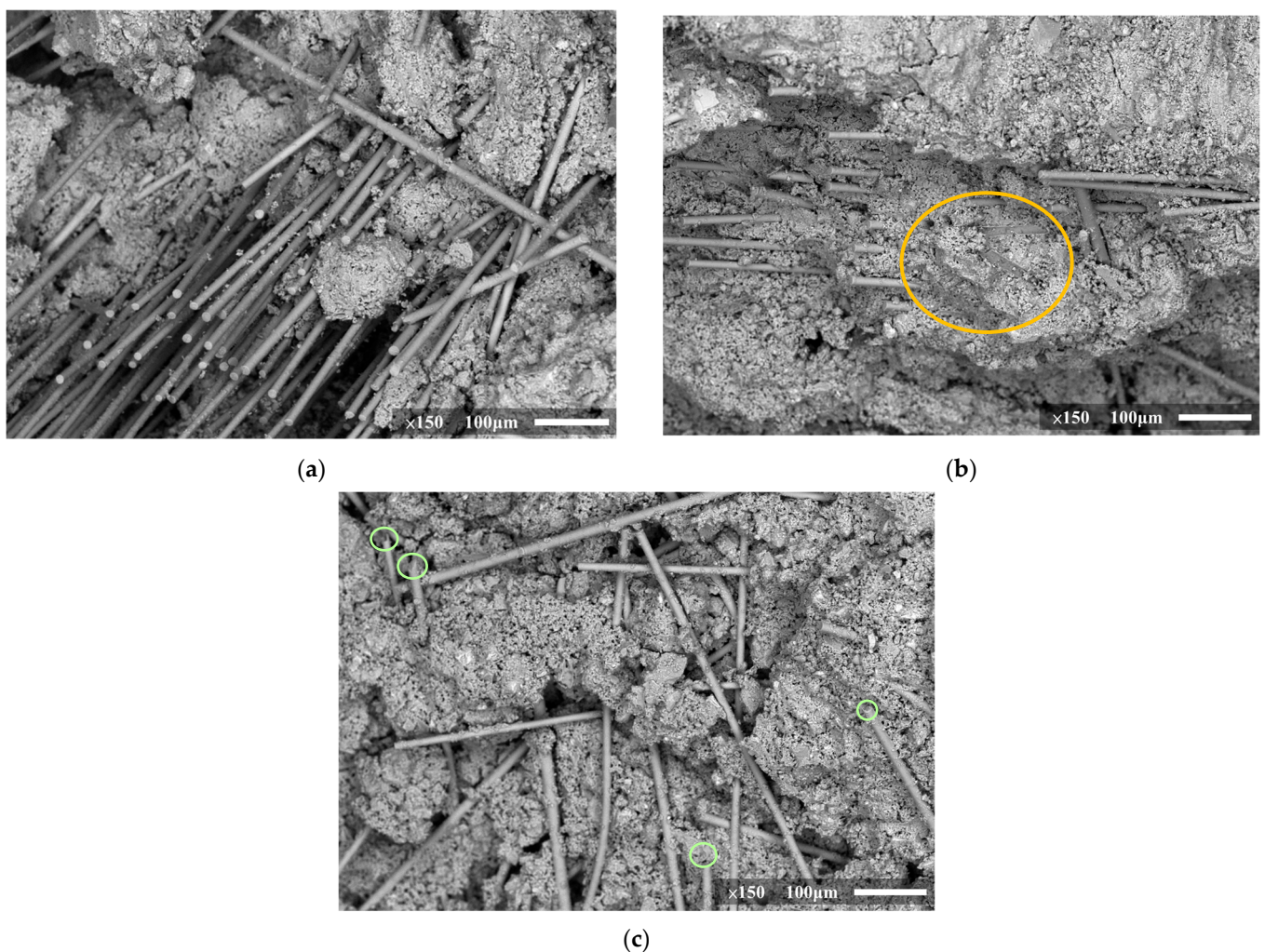


Figure 8. SEM images of a BFRC specimen after failure: (a) BFRC specimen with original basalt fiber; (b) BFRC specimen with solvent-treated basalt fiber; (c) BFRC specimen with heat-treated basalt fiber.

5. Conclusions

Based on the results of the physical–chemical properties analysis of basalt fiber and the mechanical tests of BFRC, the following conclusions can be drawn:

1. Based on a GC/MS analysis with the NIST database of extraction liquid of basalt fibers, the results showed that the two unknown substances might be “adipic acid,

- nonyl 2-octyl ester (C₂₃H₄₄O₄)” and “1,2-cyclohexanedicarboxylic acid dinonyl ester (C₂₆H₄₈O₄)”, respectively.
2. The original basalt fibers were amorphous, with no crystals or diffraction peaks in the diffraction spectrum.
 3. The SEM images indicate that the heat treatment method was more effective in removing sizing from the basalt fibers compared to the solvent treatment method.
 4. Based on the TGA mass ratio–temperature and mass ratio–time relationships of the basalt fibers, the optimal conditions for removing sizing from the surfaces of the basalt fibers were a target temperature of 300 °C and a holding time of 180 min.
 5. The SEM image observation of the failed BFRC specimens indicated that the heat-treated basalt fibers were more uniformly dispersed in the concrete than the specimens with original and solvent-treated basalt fibers.
 6. The results indicated that the mechanical properties of specimens with sizing-removed basalt fibers (HBFRC and SBFRC) were better than the specimens with original basalt fibers (OBFRC) and the benchmark specimens (B).
 7. The compressive, flexural and split tensile test results show that BFRC specimens with heat-treated basalt fibers exhibited higher strengths compared to those with original and solvent-treated basalt fibers.

Author Contributions: Conceptualization, Y.-F.L.; data curation, J.-Y.H. and S.-H.C.; formal analysis, J.-Y.H. and J.-Y.S.; funding acquisition, C.-H.H.; investigation, J.-Y.H., J.-Y.S. and S.-H.C.; methodology, Y.-F.L. and J.-Y.S.; project administration, Y.-F.L. and C.-H.H.; resources, S.-M.C. and W.-S.K.; supervision, Y.-F.L.; writing—original draft, J.-Y.H., J.-Y.S. and S.-H.C.; writing—review and editing, Y.-F.L., C.-H.H., S.-M.C. and W.-S.K. All authors have read and agreed to the published version of the manuscript.

Funding: This research was funded by the National Science and Technology Council of the Taiwan government, under contract No. NSTC 112-2221-E-027-057; and the “Research Center of Energy Conservation for New Generation of Residential, Commercial, and Industrial Sectors” from the Ministry of Education in Taiwan under contract No. L7121101-19.

Data Availability Statement: All data are contained within the article.

Conflicts of Interest: The authors declare no conflicts of interest.

References

1. Kim, J.J.; Park, G.J.; Kim, D.J.; Moon, J.H.; Lee, J.H. High-rate tensile behavior of steel fiber-reinforced concrete for nuclear power plants. *Nucl. Eng. Des.* **2014**, *266*, 43–54. [[CrossRef](#)]
2. Banthia, N.; Majdzadeh, F.; Wu, J.; Bindiganavile, V. Fiber synergy in Hybrid Fiber Reinforced Concrete (HyFRC) in flexure and direct shear. *Cem. Concr. Compos.* **2014**, *48*, 91–97. [[CrossRef](#)]
3. Mohammadi, Y.; Singh, S.P.; Kaushik, S.K. Properties of steel fibrous concrete containing mixed fibres in fresh and hardened state. *Constr. Build. Mater.* **2008**, *22*, 956–965. [[CrossRef](#)]
4. Kang, S.T.; Choi, J.I.; Koh, K.T.; Lee, K.S.; Lee, B.Y. Hybrid effects of steel fiber and microfiber on the tensile behavior of ultra-high performance concrete. *Compos. Struct.* **2016**, *145*, 37–42. [[CrossRef](#)]
5. Lou, K.; Kang, A.; Xiao, P.; Wu, Z.; Li, B.; Wang, X. Effects of basalt fiber coated with different sizing agents on performance and microstructures of asphalt mixture. *Constr. Build. Mater.* **2021**, *266*, 121155. [[CrossRef](#)]
6. Wei, B.; Song, S.; Cao, H. Strengthening of basalt fibers with nano-SiO₂–epoxy composite coating. *Mater. Des.* **2011**, *32*, 4180–4186. [[CrossRef](#)]
7. Militký, J.; Kovačič, V.; Rubnerová, J. Influence of thermal treatment on tensile failure of basalt fibers. *Eng. Fract. Mech.* **2002**, *69*, 1025–1033. [[CrossRef](#)]
8. Deák, T.; Czigány, T. Chemical composition and mechanical properties of basalt and glass fibers: A comparison. *Text. Res. J.* **2009**, *79*, 645–651. [[CrossRef](#)]
9. Xiang, Y.; Xie, Y.; Long, G. Effect of basalt fiber surface silane coupling agent coating on fiber-reinforced asphalt: From macro-mechanical performance to micro-interfacial mechanism. *Constr. Build. Mater.* **2018**, *179*, 107–116. [[CrossRef](#)]
10. Beppu, M.; Mori, K.; Ichino, H.; Muroga, Y. Local failure resistance of polypropylene fiber reinforced concrete plates subjected to projectile impact. *Int. J. Prot. Struct.* **2022**, *13*, 317–343. [[CrossRef](#)]
11. Bheel, N.; Awoyera, P.; Aluko, O.; Mahro, S.; Vilorio, A.; Sierra, C.A.S. Sustainable composite development: Novel use of human hair as fiber in concrete. *Case Stud. Constr. Mater.* **2020**, *13*, e00412. [[CrossRef](#)]

12. Li, Y.F.; Lee, K.F.; Ramanathan, G.K.; Cheng, T.W.; Huang, C.H.; Tsai, Y.K. Static and dynamic performances of chopped carbon-fiber-reinforced mortar and concrete incorporated with disparate lengths. *Materials* **2021**, *14*, 972. [[CrossRef](#)] [[PubMed](#)]
13. Li, Y.F.; Wang, H.F.; Syu, J.Y.; Ramanathan, G.K.; Tsai, Y.K. Investigating the Mechanical Performance on Static and Shock Wave Loading of Aramid Fiber-Reinforced Concrete. *Fibers* **2022**, *10*, 82. [[CrossRef](#)]
14. Li, Y.F.; Ramanathan, G.K.; Syu, J.Y.; Huang, C.H.; Tsai, Y.K. Mechanical behavior of different fiber lengths mix-proportions carbon fiber reinforced concrete subjected to static, impact, and blast loading. *Int. J. Prot. Struct.* **2022**, 20414196221138596. [[CrossRef](#)]
15. Abdellatef, M.; Heras Murcia, D.; Hogancamp, J.; Matteo, E.; Stormont, J.; Taha, M.M.R. The Significance of Multi-Size Carbon Fibers on the Mechanical and Fracture Characteristics of Fiber Reinforced Cement Composites. *Fibers* **2022**, *10*, 65. [[CrossRef](#)]
16. Mastali, M.; Dalvand, A.; Sattarifard, A. The impact resistance and mechanical properties of the reinforced self-compacting concrete incorporating recycled CFRP fiber with different lengths and dosages. *Compos. Part B Eng.* **2017**, *112*, 74–92. [[CrossRef](#)]
17. Fakharifar, M.; Dalvand, A.; Arezoumandi, M.; Sharbatdar, M.K.; Chen, G.; Kheyroddin, A. Mechanical properties of high performance fiber reinforced cementitious composites. *Constr. Build. Mater.* **2014**, *71*, 510–520. [[CrossRef](#)]
18. Li, Y.F.; Wang, H.F.; Syu, J.Y.; Ramanathan, G.K.; Tsai, Y.K.; Lok, M.H. Mechanical properties of aramid/carbon hybrid fiber-reinforced concrete. *Materials* **2021**, *14*, 5881. [[CrossRef](#)]
19. Li, Y.F.; Yang, K.H.; Hsu, P.Y.; Syu, J.Y.; Wang, S.J.; Kuo, W.S.; Tsai, Y.K. Comparing Mechanical Characterization of Carbon, Kevlar, and Hybrid-Fiber-Reinforced Concrete under Quasistatic and Dynamic Loadings. *Buildings* **2023**, *13*, 2044. [[CrossRef](#)]
20. Palanisamy, E.; Ramasamy, M. Dependency of sisal and banana fiber on mechanical and durability properties of polypropylene hybrid fiber reinforced concrete. *J. Nat. Fibers* **2022**, *19*, 3147–3157. [[CrossRef](#)]
21. Ganta, J.K.; Rao, M.S.; Mousavi, S.S.; Reddy, V.S.; Bhojaraju, C. Hybrid steel/glass fiber-reinforced self-consolidating concrete considering packing factor: Mechanical and durability characteristics. *Structures* **2020**, *28*, 956–972. [[CrossRef](#)]
22. Teja Prathipati, S.R.R.; Rao, C.B.K. A study on the uniaxial behavior of hybrid graded fiber reinforced concrete with glass and steel fibers. *Mater. Today Proc.* **2020**, *32*, 764–770. [[CrossRef](#)]
23. Thomason, J.L. Glass fibre sizing: A review. *Compos. Part A Appl. Sci. Manuf.* **2019**, *127*, 105619. [[CrossRef](#)]
24. Ralph, C.; Lemoine, P.; Boyd, A.; Archer, E.; McIlhagger, A. The effect of fibre sizing on the modification of basalt fibre surface in preparation for bonding to polypropylene. *Appl. Surf. Sci.* **2019**, *475*, 435–445. [[CrossRef](#)]
25. Gorowara, R.L.; Kosik, W.E.; McKnight, S.H.; McCullough, R.L. Molecular characterization of glass fiber surface coatings for thermosetting polymer matrix/glass fiber composites. *Compos. Part A Appl. Sci. Manuf.* **2001**, *32*, 323–329. [[CrossRef](#)]
26. Iorio, M.; Santarelli, M.L.; González-Gaitano, G.; González-Benito, J. Surface modification and characterization of basalt fibers as potential reinforcement of concretes. *Appl. Surf. Sci.* **2018**, *427*, 1248–1256. [[CrossRef](#)]
27. Thomason, J. A review of the analysis and characterisation of polymeric glass fibre sizings. *Polym. Test.* **2020**, *85*, 106421. [[CrossRef](#)]
28. Li, Y.F.; Li, J.Y.; Ramanathan, G.K.; Chang, S.M.; Shen, M.Y.; Tsai, Y.K.; Huang, C.H. An experimental study on mechanical behaviors of carbon fiber and microwave-assisted pyrolysis recycled carbon fiber-reinforced concrete. *Sustainability* **2021**, *13*, 6829. [[CrossRef](#)]
29. Li, Y.F.; Yang, T.H.; Kuo, C.Y.; Tsai, Y.K. A Study on improving the mechanical performance of carbon-fiber-reinforced cement. *Materials* **2019**, *12*, 2715. [[CrossRef](#)]
30. Li, Y.F.; Li, J.Y.; Syu, J.Y.; Yang, T.H.; Chang, S.M.; Shen, M.Y. Mechanical Behaviors of Microwave-Assisted Pyrolysis Recycled Carbon Fiber-Reinforced Concrete with Early-Strength Cement. *Materials* **2023**, *16*, 1507. [[CrossRef](#)]
31. Thomason, J.L.; Nagel, U.; Yang, L.; Bryce, D. A study of the thermal degradation of glass fibre sizings at composite processing temperatures. *Compos. Part A Appl. Sci. Manuf.* **2019**, *121*, 56–63. [[CrossRef](#)]
32. Jenkins, P.G.; Yang, L.; Liggat, J.J.; Thomason, J.L. Investigation of the strength loss of glass fibre after thermal conditioning. *J. Mater. Sci.* **2015**, *50*, 1050–1057. [[CrossRef](#)]
33. Wang, Z.T.; Luo, H.J.; Zhang, J.; Chen, H.W.; Zhang, L.; Wu, L.L.; Jiang, H. Water-soluble polysiloxane sizing for improved heat resistance of basalt fiber. *Mater. Chem. Phys.* **2021**, *272*, 125024. [[CrossRef](#)]
34. Overkamp, T.; Mahltig, B.; Kyosev, Y. Strength of basalt fibers influenced by thermal and chemical treatments. *J. Ind. Text.* **2018**, *47*, 815–833. [[CrossRef](#)]
35. Li, Y.F.; Hung, J.Y.; Syu, J.Y.; Chang, S.M.; Kuo, W.S. Influence of sizing of basalt fiber on the mechanical behavior of basalt fiber reinforced concrete. *J. Mater. Res. Technol.* **2022**, *21*, 295–307. [[CrossRef](#)]
36. Frey, M.; Brunner, A.J. Assessing glass-fiber modification developments by comparison of glass-fiber epoxy composites with reference materials: Some thoughts on relevance. *Proc. Inst. Mech. Eng. Part L J. Mater. Des. Appl.* **2017**, *231*, 49–54. [[CrossRef](#)]
37. Guo, X.; Lu, Y.; Sun, Y.; Wang, J.; Li, H.; Yang, C. Effect of sizing on interfacial adhesion property of glass fiber-reinforced polyurethane composites. *J. Reinf. Plast. Compos.* **2018**, *37*, 321–330. [[CrossRef](#)]
38. Feih, S.; Wei, J.; Kingshott, P.; Sørensen, B.F. The influence of fibre sizing on the strength and fracture toughness of glass fibre composites. *Compos. Part A Appl. Sci. Manuf.* **2005**, *36*, 245–255. [[CrossRef](#)]
39. Jiang, S.; Li, Q.; Zhao, Y.; Wang, J.; Kang, M. Effect of surface silanization of carbon fiber on mechanical properties of carbon fiber reinforced polyurethane composites. *Compos. Sci. Technol.* **2015**, *110*, 87–94. [[CrossRef](#)]
40. Tanoglu, M.; Ziaee, S.; Mcknight, S.H.; Palmese, G.R.; Gillespie, J.W. Investigation of properties of fiber/matrix interphase formed due to the glass fiber sizings. *J. Mater. Sci.* **2001**, *36*, 3041–3053. [[CrossRef](#)]

41. Thomason, J.L. The interface region in glass fibre-reinforced epoxy resin composites: 3. Characterization of fibre surface coatings and the interphase. *Composites* **1995**, *26*, 487–498. [[CrossRef](#)]
42. Moosburger-Will, J.; Bauer, M.; Laukmanis, E.; Horny, R.; Wetjen, D.; Manske, T.; Schmidt-Stein, F.; Töpker, J.; Horn, S. Interaction between carbon fibers and polymer sizing: Influence of fiber surface chemistry and sizing reactivity. *Appl. Surf. Sci.* **2018**, *439*, 305–312. [[CrossRef](#)]
43. ASTM D3822-07; Standard Test Method for Tensile Properties of Single Textile Fibers. ASTM: West Conshohocken, PA, USA, 2007.
44. ASTM C33/C33M-18; Standard Specification for Concrete Aggregates. ASTM: West Conshohocken, PA, USA, 2018.
45. ASTM C39/C39M-01; Standard Test Method for Compressive Strength of Cylindrical Concrete Specimens. ASTM: West Conshohocken, PA, USA, 2001.
46. ASTM C293/C293M-16; Standard Test Method for Flexural Strength of Concrete. ASTM: West Conshohocken, PA, USA, 2016.
47. ASTM C496/C496M-17; Standard Test Method for Splitting Tensile Strength of Cylindrical Concrete Specimens. ASTM: West Conshohocken, PA, USA, 2017.
48. Ku-Herrera, J.J.; Avilés, F.; Nistal, A.; Cauch-Rodríguez, J.V.; Rubio, F.; Rubio, J.; Bartolo-Pérez, P. Interactions between the glass fiber coating and oxidized carbon nanotubes. *Appl. Surf. Sci.* **2015**, *330*, 383–392. [[CrossRef](#)]
49. Britcher, L.G.; Kehoe, D.; Matisons, J.G. Direct spectroscopic measurements of adsorption of siloxane polymers onto glass fiber surfaces. In *Silanes and Other Coupling Agents*; Mittal, K.L., Ed.; CRC Press: London, UK, 2020; Volume 2, pp. 99–114.
50. Chang, J.H.; Tsai, Y.S.; Yang, P.Y. A Review of Glass Fibre Recycling Technology Using Chemical and Mechanical Separation of Surface Sizing Agents. *Recycling* **2021**, *6*, 79. [[CrossRef](#)]
51. Chakartnarodom, P.; Prakaypan, W.; Ineure, P.; Chuankrerkkul, N.; Laitila, E.A.; Kongkajun, N. Properties and performance of the basalt-fiber reinforced texture roof tiles. *Case Stud. Constr. Mater.* **2020**, *13*, e00444. [[CrossRef](#)]
52. Bindiganavile, V.S. Dynamic Fracture Toughness of Fiber Reinforced Concrete. Ph.D. Thesis, University of British Columbia, Vancouver, BC, Canada, 2003.
53. Demirboga, R.; Farhan, K.Z. Palm oil fuel ash (POFA). In *Sustainable Concrete Made with Ashes and Dust from Different Sources*; Rafat, S., Rafik, B., Eds.; Woodhead Publishing: Sawston/Cambridge, UK, 2022; Chapter 7; pp. 279–330.

Disclaimer/Publisher’s Note: The statements, opinions and data contained in all publications are solely those of the individual author(s) and contributor(s) and not of MDPI and/or the editor(s). MDPI and/or the editor(s) disclaim responsibility for any injury to people or property resulting from any ideas, methods, instructions or products referred to in the content.